**Annales
Geophysicae**

Disruption of magnetospheric current sheet by quasi-electrostatic field

W. W. Liu and J. Liang

Space Science Branch, Canadian Space Agency, Canada

Abstract. Recent observational evidence has indicated that local current sheet disruptions are excited by an external perturbation likely associated with the kinetic ballooning (KB) instability initiating at the transition region separating the dipole- and tail-like geometries. Specifically a quasi-electrostatic field pointing to the neutral sheet was identified in the interval between the arrival of KB perturbation and local current disruption. How can such a field drive the local current sheet unstable? This question is considered through a fluid treatment of thin current sheet (TCS) where the generalized Ohm's law replaces the frozen-in-flux condition. A perturbation with the wavevector along the current is applied, and eigenmodes with frequency much below the ion gyrofrequency are sought. We show that the second-order derivative of ion drift velocity along the thickness of the current sheet is a critical stability parameter. In an E-field-free Harris sheet in which the drift velocity is constant, the current sheet is stable against this particular mode. As the electrostatic field grows, however, potential for instability arises. The threshold of instability is identified through an approximate analysis of the theory. For a nominal current sheet half-thickness of 1000 km, the estimated instability threshold is $E \sim 4$ mV/m. Numerical solutions indicate that the two-fluid theory gives growth rate and wave period consistent with observations.

Keywords. Magnetospheric physics (Electric fields; MHD waves and instabilities; Plasma sheet)

1 Introduction

Thin current sheets (TCSs) are widely observed in natural plasma systems from the solar corona to Earth's magnetotail, especially as a precursor to eruptive episodes of global

energy release. In the magnetosphere, TCSs mainly manifest themselves as embedded structures in the central plasma sheet (CPS) during the growth phase of substorm (Sergeev et al., 1993; Pulkkinen et al., 1999). As convection in the magnetotail intensifies, energy cannot flow around or through the largely dipolar inner magnetosphere in sufficient quantity to balance the input from the distant tail, and the accumulated energy in the CPS stretches the magnetic field tailward. Formation of thin current sheets starts out as a quasistatic process, taking tens of minutes to develop in the magnetosphere. Evolution and maintenance of TCSs has been a subject of extensive investigation through theory and simulation (Lee et al., 1995; Pritchett and Coroniti, 1995; Schindler and Birn, 2002; Sitnov et al., 2000; Birn et al., 2004).

TCSs are also known to be highly dynamic, collapsing rapidly in a matter of seconds and leading to the expansion of substorms. Why some TCSs are meta-stable while others not is a question lacking a satisfactory answer. Many researchers take the thickness of a TCS as the determining factor in the stability question. TCSs are often observed to have a thickness comparable to ion gyroradius ($\sim$1000 km); at this scale, magnetic field can slip through the ion fluid owing to the breakdown of the frozen-in-flux condition. Yet, some TCSs can persist in this condition for many minutes, far longer than the time it takes for information to propagate through the current sheet via the fast mode, while other TCSs, for roughly the same integrated current strength and thickness, are unstable, losing equilibrium in tens of seconds. Therefore, there could be factors other than thickness at play.

Recent observations have shed new light on the problem. Saito et al. (2008a, b) showed that local current disruptions (CDs) are preceded by several minutes of wave activity in the 10–20 mHz range, which they attributed to the ballooning instability. Through multiple satellite observations, Donovan et al. (2008) and Liu et al. (2008) showed that the 10–20 mHz wave band propagates downtail at a substantially reduced speed compared to the fast mode. Through a wavelet

analysis, Liu et al. (2008) and Liang et al. (2009) were able to identify that the mode directly responsible for local CD was not the KB mode but a new mode (referred to as the CD mode) occurring at a higher frequency in the 20–100 mHz range. Liu et al. (2008) demonstrated that the CD mode was quasi-electrostatic. The above studies give us sufficient reason to believe that waves in the 20–100 mHz range play a significant role in local CDs. Using independent techniques, Saito et al. (2008a) and Liang et al. (2008) estimated the azimuthal wavelength of the waves to be 600–3000 km, comparable to the ion thermal gyroradius in equatorial plane.

We first review some essential information and key arguments regarding the formation and nature of the quasi-electric field (QEF) before onset. We then consider an idealized thin current sheet represented by the Harris distribution. We will show that this configuration is stable in the two-fluid regime no matter how thin it is. We then introduce an electrostatic field in the equation and illustrate its propensity to drive the system toward instability. The instability threshold is established through an approximate analysis of the eigenvalue equation. Numerical examples are presented to demonstrate that the predictions of the theory are in line with observed growth time and oscillating periods. Contrast is drawn between the new instability and previously known drift-kink instability. How the theory fits in the larger context and some of its limitations are described in the discussion section.

2   Quasi-electrostatic field in a thin current sheet

Numerous studies have shown that the thickness of the near-Earth current sheet can become comparable to the ambient ion gyroradius (Mitchell et al., 1990; Sergeev et al., 1993; Sanny et al., 1994). On this scale, ions are partially demagnetized and do not fully follow the magnetic field lines, while electrons, by and large, continue to be frozen in the **B** field. In this condition, charge separation may develop in the neutral sheet.

The existence of a QEF in a TCS has been studied theoretically (Schindler and Birn, 2002; Birn et al., 2004) and found in computer simulations (e.g., Pritchet and Coroniti, 1995). Its latest experimental identification, particularly its association with local CDs, was reported by Liu et al. (2008). Using different techniques, Liang et al. (2008) and Saito (2008a) showed that the wave mode associated with substorm onset has a dominant azimuthal wavelength on the order of 1000 km. In-situ and THEMIS ASI observations gave the growth timescale of the mode in the 10–30 s range (Liang et al., 2008). Coupled with in-situ magnetic measurements reported in Liu et al. (2008), the curl of the electric field can be estimated through Faraday's law. The resulting $|\nabla \times \boldsymbol{E}|$ was found to be small compared to the measured electric field over the estimated length scale. The observed electric field had a neutral sheet-pointing bias, implying a negative charging of the neutral sheet. The electric field was found only

in the interval between the arrival of the kinetic ballooning perturbation and onset of local CD and subsided quickly afterward, whereas the magnetic field perturbation persisted for many minutes further. The interpretation was that the local CD removed the condition for charge imbalance and quenched the electrostatic field.

From both theory and observations, the existence of a QEF before local CD appears to be well established. What is not clear is whether the QEF is an incidental property or an essential element in the destabilization of the local current sheet. In the following sections, we prove that the latter is possible.

3   Theory

3.1   Context

In order to see where our theory stands and that the result indeed represents a new mode, a brief survey of the extant literature is conducted. The survey is not meant to be comprehensive, but to draw out the necessary contrast with some known modes of TCS instability. Dalburgh et al. (1992) showed that the classical Harris sheet with $B_z=0$ is stable against ideal MHD perturbations. However, in the presence of a finite B_z, the problem of current sheet stability becomes more complicated. Various authors have studied the ballooning mode associated with field line curvature under the MHD and kinetic conditions (Hameiri et al., 1991; Roux et al., 1991; Liu, 1997; Cheng and Lui, 1998). As we will comment in the discussion, the presence of B_z can further introduce resonant and non-local plasmas responses that may not be accounted for in a fluid treatment.

The two-fluid theory is a more accurate approximation of plasma physics in a TCS. A much studied two-fluid mode is the drift-kink instability (DKI). Under the fictitious condition $m_i=m_e$ and $T_i=T_e$ (where the subscripts i and e refer to the ion and electron species, respectively), Pritchett et al. (1996) derived the growth rate of DKI in the classical Harris sheet as

$$\gamma = k_y V_0 \left(1 - \frac{2k_y V_0}{\Omega_0}\right) \tag{1}$$

where $2V_0$ is the relative drift between the two species, k_y the wavenumber parallel to the drift, and Ω_0 the gyrofrequency in the asympotic field of the Harris sheet. Numerical calculations and simulations of these authors indicate that the growth rate decreases as more realistic mass ratio is used.

Daughton (1999) studied the DKI mode under the condition of incompressibility for an unmagnetized inner region but without assuming identical ion and electron properties. The growth rate was derived to be

$$\gamma = \frac{k_y V_{0i}}{1 + m_e/m_i} \left(1 + \frac{T_e}{T_i}\right) \sqrt{\frac{m_e}{m_i}} \tag{2}$$

Equation (2) suggests that the DKI is an electron inertial effect, as well as a relative drift effect.

Lapenta and Brackill (1999) constructed a kinetic model of DKI, again under some approximations. Their results were largely consistent with those of Pritchett et al. (1996) and Daughton (1999).

In order to clearly distinguish our theory from DKI, we take the limit $m_e=0$. By virtue of Eq. (2), this limit should eliminate the DKI from our consideration, and whatever mode that emerges should thus be different.

We note that numerous other TCS modes have been studied in the literature. They often involve kinetic processes in the velocity space. While these modes are potentially important, they do not have a close relationship to what interests us here, namely TCS modes arise in a fluid formulation of the plasma physics.

3.2 Hall MHD formulation

A key motivation for the present work is an observation of the implication of the limits made by Pritchett et al. (1996) and Daughton (1999). It is well-known that a linear combination of the momentum equations of the ion and electron species in the two fluid theory results in the generalized Ohm's law (GOL) (e.g., Krall and Trivelpiece, 1973). When the ion and electron masses are made equal artificially as in Pritchett et al. (1996), the Hall term in GOL vanishes, resulting in a loss of important physics. In the Daughton approximation, the ion and electron fluids are incompressible in the unmagnetized region. It can be verified that this condition is not satisfied generally in our treatment. Thus, the mode of interest here, which we call the Hall mode, was not captured by the Daughton limit.

In-situ observations have shown that the electron temperature T_e is typically much lower than the ion temperature in TCSs in the magnetosphere. As a further simplification, we take the limit $T_e \to 0$. The role of electrons in our theory is to provide the negative charge to achieve quasi-neutrality, but otherwise have no impact on the mode under study. The generalized Ohm's law under our approximations is written as

$$E = -u \times B + \frac{J \times B}{ne} \tag{3}$$

where E the electric field, u is the plasma velocity, B the magnetic field, J the electric current density, n the plasma density, and e the unit electric charge. Equation (3) replaces the ideal MHD condition $E=-u \times B$. Depending on one's preference, our theory can be regarded either as a reduced version of the two-fluid theory (through the $m_e \to 0$ and $T_e \to 0$ limits) or a generalized version of one-fluid MHD (through the Hall MHD condition 3).

For mathematic convenience, Eq. (3) is combined with the momentum equation

$$\rho \left(\frac{\partial u}{\partial t} + u \cdot \nabla u \right) = -\nabla p + \frac{J \times B}{ne} \tag{4}$$

to give an alternate form of the GOL as

$$E + u \times B = \frac{m}{e} \left(\frac{\partial u}{\partial t} + u \cdot \nabla u \right) + \frac{\nabla p}{ne} \tag{5}$$

The mass conservation, energy equation, and Faraday's law, written in the stated order below, round out the equations

$$\frac{\partial \rho}{\partial t} = -\rho \nabla \cdot u - u \cdot \nabla \rho \tag{6}$$

$$\frac{\partial p}{\partial t} = -\lambda p \nabla \cdot u - u \cdot \nabla p \tag{7}$$

$$\frac{\partial B}{\partial t} = -\nabla \times E \tag{8}$$

where ρ the plasma mass density ($\rho=nm$, with m being the ion mass), p the plasma pressure, and λ the polytropic index. In the ideal MHD, λ is usually assigned the value 5/3, corresponding to the isotropic adiabatic compression. In the two-fluid regime, ions are partially decoupled from the magnetic field and do not respond to its variation as rigidly as in the ideal MHD regime; a λ value closer to unity may be justified. In fact, the Harris sheet has the property $p/n=$const, consistent with a polytropic index of 1. Without affecting the generality of the argument and result, we set $\lambda=1$ in this study.

Using the vector identity $u \cdot \nabla u = \nabla \left(u^2/2 \right) - u \times \nabla \times u$ and defining a pseudo-magnetic field $H=B+m\nabla \times u/e$, we obtain from Eqs. (5) and (8) the following

$$\frac{\partial H}{\partial t} = H \cdot \nabla u - H \nabla \cdot u - u \cdot \nabla H + \frac{1}{e} \nabla p \times \nabla \frac{1}{n} \tag{9}$$

Equations (4), (6), (7), and (9) form a closed set. In the Appendix, we describe the linearization of these equations and the derivation of the eigenvalue equation. Thevalidity of the fluid treatment will be justified in the discussion section.

The background magnetic configuration is the classical Harris sheet, with $B_z=0$ and the following distributions:

$$B_x = B_0 \tanh \left(\frac{z}{L} \right) \tag{10}$$

$$n = \frac{p_0}{T_0 \cosh^2 (z/L)} \tag{11}$$

$$p = \frac{p_0}{\cosh^2 (z/L)} \tag{12}$$

where L is the half-thickness of the current sheet, T_0 is the ion temperature, and $p_0=B_0^2/2\mu_0$.

We assume that the wave mode is dominated by the azimuthal wavenumber k_y. This approximation is motivated by the observations of Saito et al. (2008a) and Liang et al. (2008) that the azimuthal wavelength has the order of $\sim$1000 km, likely short in comparison with the radial extent of current disruption ($\geq 1 R_E$). For this reason, the linear mode under consideration has the harmonic form $f(z) \exp i \left(k_y y - \omega t \right)$

throughout this study. Note that DKI perturbations have the same harmonic form.

In the Harris sheet, the plasma has a zeroth-order velocity in the y direction given by

$$U = \frac{1}{\mu_0 en} \frac{dB_x}{dz} + \frac{E_z}{B_x} = \frac{2T_0}{eLB_0} + \frac{E_z}{B_0 \tanh(z/L)} \quad (13)$$

where E_z is the zeroth-order electrostatic field discussed in Sect. 2. In the classical Harris sheet, the ion and electron drifts are balanced in proportion to the temperature, i.e., $U_i/T_i + U_e/T_e = 0$, and $E_z = 0$. However, we have noted in Sect. 2 that, when ion-scale effects become significant, this balance may be broken leading to a finite E_z.

We begin the study by considering the Harris sheet without E_z. This is a reasonable approximation during periods when the current sheet is relatively thick and consistent with the configuration underlying the DKI studies cited above. Since U=const (hence U'=0) in this case, the linear mode is described by a relatively simple equation

$$\frac{\partial}{\partial z}\left(\frac{1}{\rho}\frac{\partial \rho \Delta u_y}{\partial z}\right) + \left(\frac{\omega_d^2}{c_f^2} - k_y^2 + \frac{mB_x k_y}{\mu_0 e\rho^2 c_f^2}\frac{d\rho}{dz}\omega_d\right)\Delta u_y = 0 \quad (14)$$

whose derivation and definition of terms therein is given in the Appendix. Multiplying the complex conjugate $\rho \Delta u_y*$ to Eq. (14) and integrating over z, we obtain the following equation, under the regularity condition $\Delta u_y(z=\pm\infty) = du_y(z=\pm\infty)/dz = 0$,

$$A_1\omega_d^2 + A_2\omega_d + A_3 = 0 \quad (15)$$

where

$$A_1 = \int_{-\infty}^{\infty} \frac{\rho}{c_f^2}|\Delta u_y|^2 \, dz \quad (16)$$

$$A_2 = \int_{-\infty}^{\infty} \frac{B_x k_y}{\mu_0 e\rho c_f^2}\frac{d\rho}{dz}|\Delta u_y|^2 \, dz \quad (17)$$

$$A_3 = -\int_{-\infty}^{\infty}\left[\frac{1}{\rho}\left|\frac{\partial \rho \Delta u_y}{\partial z}\right|^2 + k_y^2\rho|\Delta u_y|^2\right]dz \quad (18)$$

The solution to Eq. (15) is

$$\omega_d = \frac{-A_2 \pm \sqrt{A_2^2 - 4A_1 A_3}}{2A_1} \quad (19)$$

Since A_1 is by definition positive, and A_3 by definition negative, the eigenfrequencies given by Eq. (19) are always real, and the two-fluid modes for the E-field-free Harris sheet are thus always stable.

It is pertinent to comment that both analytic and simulation results show that the DKI is unstable in a classical Harris

sheet without E_z. In this regard, one can conclude that the DKI is more easily excited than the Hall mode.

When U is not a constant of space, however, the Hall mode can become unstable and can achieve a faster growth rate than the DKI (as our later numerical calculation will attest). The eigenvalue equation of the linear mode is more involved under this condition. The derivation of this equation is described in the Appendix, culminating in the form

$$\frac{d}{dz}\frac{\rho}{k_y - \omega_d F(z)}\frac{d\Delta u_z}{dz} + \left[\frac{k_y}{\omega_d}\frac{d}{dz}\left[\left(\frac{\rho}{k_y - \omega_d F}\right)\frac{dU}{dz}\right] - \rho k_y\right]\Delta u_z = 0 \quad (20)$$

where

$$F(z) = \frac{\omega_d}{k_y c_f^2} + \frac{mB_x(z)}{\mu_0 e\rho^2}\frac{d\rho}{dz} \quad (21)$$

Equation (20) lacks an energy-principle integral to give a general perspective on the stability problem as in Eq. (14). An approximate but instructive look at the problem, however, can be effected by examining the near-solution to the equations near the neutral sheet, namely, for $z \ll L$. In this limit, odd functions B_x, dp/dz, and dU/dz can be neglected in comparison to even functions such as dB_x/dz, U, and d^2U/dz^2. Writing $d^2\Delta u_z/dz^2 = -k_n^2\Delta u_z$, we obtain from the near-field equation

$$G(\omega_d) = \omega_d\left(\omega_d^2 - k_\perp^2 c_f^2\right) = k_y c_f^2 \frac{d^2U}{dz^2} \quad (22)$$

where $k_\perp^2 = k_y^2 + k_n^2$. It is understood that all terms in Eq. (22) are evaluated at the neutral sheet z=0. Consider the symmetric mode $\Delta u_y(0) = 1$ and $\Delta u_z(0) = 0$. This boundary condition leads to unique solutions to Eq. (20). It can also be verified that asymptotically at $z \to \infty$, the solution varies as $C_1\exp(k_y z) + C_2\exp(-k_y z)$. Only for discrete values of k_n can the physical constraint C_1=0 be satisfied. As a rough guide, if we match the near solution $\Delta u_y = A\cos(k_n z)$ and far solution $C_2\exp(-k_y z)$ at z=L, we find $k_n + k_y\tan(k_n L) = 0$, which gives a discrete set of k_n values.

When the second derivative of the drift velocity is significant, the possibility of instability arises. The situation is visualized through Fig. 1. We note that $G(\omega_d) = 0$ has real solutions $\omega_\Delta = 0$ and $\omega_\Delta = \pm k_\perp c_f$, the latter being the fast mode. For solutions to the equation $G(\omega_d) = C$, however, it is clear that for C outside the stable range marked in Fig. 1, the equation has only one real solution, and the other two is a pair of conjugate complex numbers, one of which is unstable. It can be easily verified that the unstable situation occurs first when C exceeds the local maximum of $G(\omega_d)$, occurring at

$$\omega_m = -\frac{1}{\sqrt{3}}k_\perp c_f \quad (23)$$

with value

$$G_{max} = \frac{2}{3\sqrt{3}}k_\perp^3 c_f^3 \quad (24)$$

From the above argument, it is easily verified that

$$\frac{d^2U}{dz^2} > \frac{2k_\perp^3 c_f}{3\sqrt{3}k_y} \tag{25}$$

is a necessary condition of instability. Equation (22) can be rearranged to the following form,

$$(\omega_d - \omega_m)^2 (\omega_d - \omega_L) = k_y c_F^2 \frac{d^2U}{dz^2} - \frac{2k_\perp^3 c_F^3}{3\sqrt{3}} \tag{26}$$

where

$$\omega_L = \frac{2}{\sqrt{3}} k_\perp c_f \tag{27}$$

When the TCS distribution just passes the threshold of instability, the frequency can be written as $\omega_\Delta = \omega_m + i\gamma$, which, upon substitution into Eq. (26), yields

$$\gamma = \pm \frac{1}{3^{1/4}} \sqrt{\frac{k_y c_F}{k_\perp}} \left[\frac{d^2U}{dz^2} - \frac{2k_\perp^3 c_F}{3k_y \sqrt{3}} \right]^{1/2} \tag{28}$$

It can be confirmed that the unstable mode given in Eq. (28) exists only for intermediate values of k_y; namely, in both the $k_y \to 0$ and $k_y \to \infty$ limits, $\omega_i = 0$. If we assume that $k_n = \alpha/H$ is reasonably insensitive to k_y, the stabilizing term on the right-hand side of Eq. (28) minimizes at

$$k_y = \frac{k_n}{\sqrt{2}} \tag{29}$$

At this k_y value,

$$\gamma = 0.69 c_F^{1/2} \left[\frac{d^2U}{dz^2} - \frac{k_n^2}{2} c_F \right]^{1/2} \tag{30}$$

Note that there is another branch of instability for the local minimum in Fig. 1. Using the same procedure as above, one can show that this branch has a growth rate given by Eq. (28) but with the sign of the d^2U/dz^2 term reversed.

From Eq. (13), we see that U can become a variable of space either due to the emergence of E_z or due to the variation of the temperature along z. We consider the E_z effect first. Assume the electric field has the form,

$$E_z = -\frac{E_0 z}{L} \exp\left(-\frac{z^2}{L^2}\right) \tag{31}$$

Substituting Eq. (31) into (30) gives the critical value

$$E_0 \sim \frac{3B_0 c_F}{8} \tag{32}$$

for $k_n \sim 1/L$. The maximum E_z value according to Eq. (3) is $E_0/\sqrt{2e}$. If we take $B_0 = 50$ nT and neutral-sheet density $n_0 = 1$ cm^{-3}, we obtain $c_F \sim 700$ km/s, giving $E_z \sim 4$ mV/m as the instability threshold. In Liu et al. (2008), the average E_z value reached 4 mV/m in the few minutes prior to onset, with spikes at high as 10 mV/m.
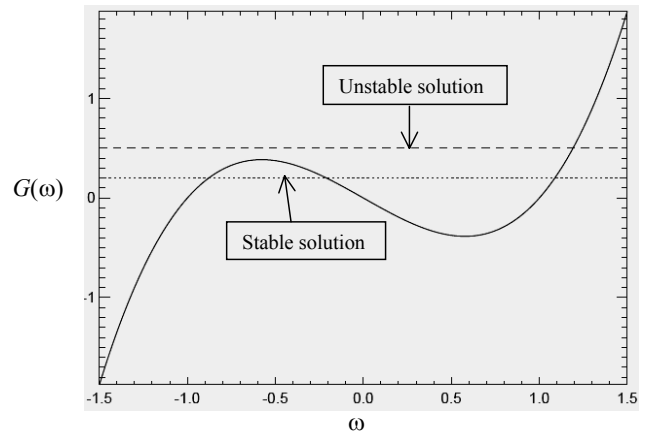
Fig. 1. Diagram showing the development of instability. $G(\omega)$ is the function given in Eq. (28). The figures shows the change of the solution to $G(\omega) = C$. When C is sufficiently large (dashed line), there is a pair of complex solution, one of which is unstable.

4 Numerical solutions

Equations (20) are solved numerically as an eigenvalue problem to expand on the analysis given in the last section. The calculations were performed under realistic parameters, and the results are then compared to actual observations. We concentrate on the case of symmetric mode $\Delta u_z (z=0) = 0$ and $d\Delta u_z (z=0)/dz = 0$. The shooting method is used to search for the eigenvalue ω, under the constraint $\Delta u_z (z \to \infty) = 0$. As a test and for curiosity, we applied the algorithm to the field-free Harris sheet and indeed found no unstable mode.

The first case deals with the E_z-driven mode, with the distribution given by Eq. (31). The background distributions are show in Fig. 2a. Figure 2b gives one example of eigenvalue solutions as a function of the azimuthal wavelength $\lambda_y = 2\pi/k_y$, for the following parameters: $n_0 = 1$ cm^{-3}, $B_0 = 50$ nT, $E_{z\max} = 5$ mV/m, and $L = 1000$ km. The real part of the eigen-period has the range 20–40 s, and the imaginary part (expressed as growth time) is approximately constant, at 15–18 s. These values are consistent with the period of CD mode from wavelet analysis of Liu et al. (2008) and Liang et al. (2008), and the growth timescale of CD we reported earlier (Donovan et al., 2008; Liang et al., 2008).

We remark that the instability is sensitive to E_z and L. Our search algorithm has an upper limit of 90 s for the growth time. For $E_{z\max} < 2$ mV/m, and $H > 3000$ km, there is no unstable mode returned by the algorithm within the search space. The numerical results are consistent with our analysis given in Sect. 3.

In Fig. 3, we present a comparative case on how the instability is also possible when there is a temperature variation across the current sheet, in the absence of E_z. The temperature model is given by

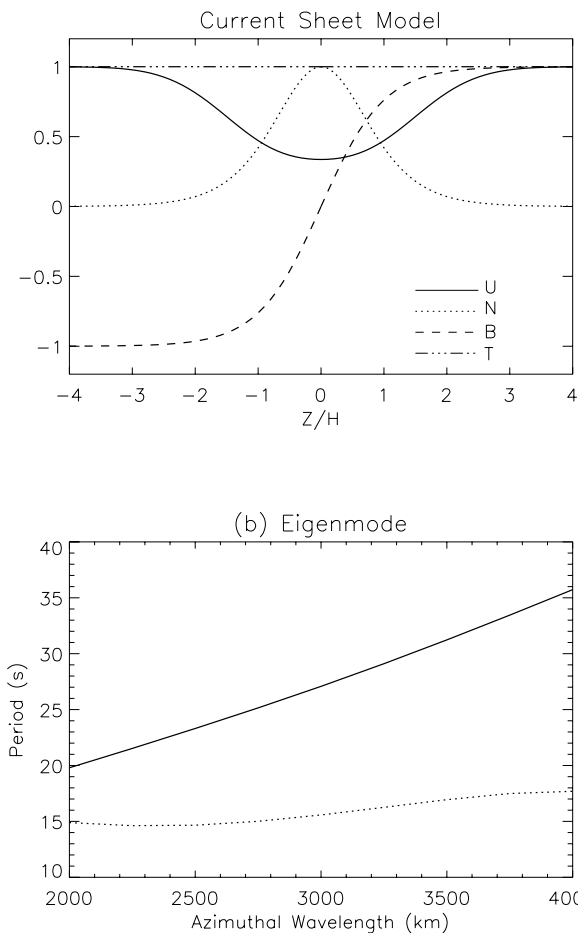$$T(z), \ U(z) \propto \cosh^{2/\lambda - 2}\left(\frac{z}{H}\right) \tag{33}$$

Fig. 2. Numerical solution of the unstable eigenmode for the case given in Eq. (37) and parameters given the subsequent text. Plot **(a)** shows the variation of the background quantities of the model current sheet. Plot **(b)** gives the real (solid) and imaginary (dotted) parts of the eigenvalue as a function of azimuthal wavelength.
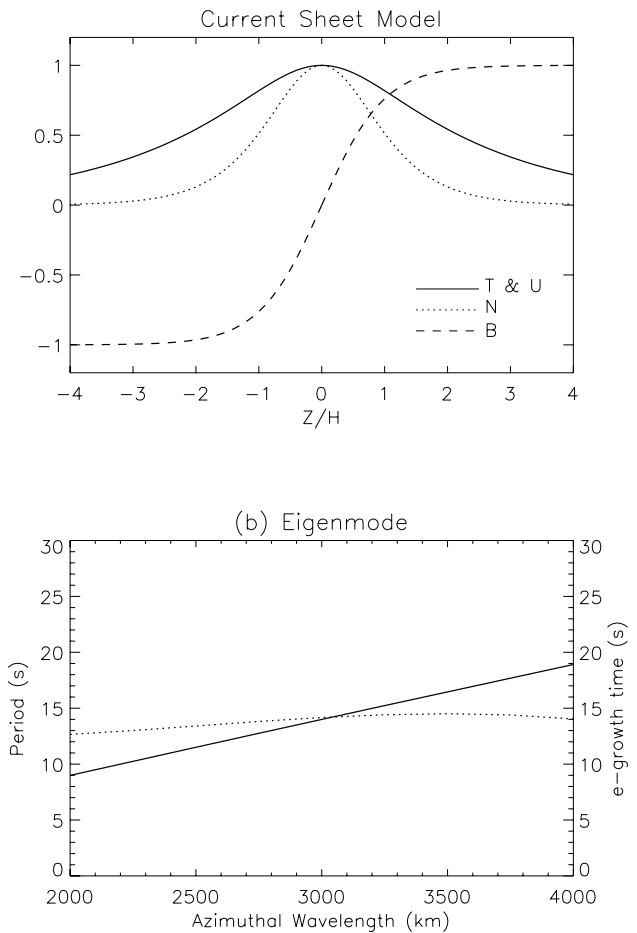
Fig. 3. Same as Fig. 2, but for the variable temperature model given in Eq. (39). The quasi-electrostatic field is absent in this calculation.

We chose $\lambda=1.3$ in the example shown in Fig. 3. In Fig. 3a, the background distributions are plotted. In contrast to Fig. 2a, $d^2U/dz^2<0$ in the neutral sheet. We showed previously that both large positive and negative values of the second-order derivative of U can lead to instability. The variation of the eigenvalue as a function of λ_y is shown in Fig. 3b, for the same set of background parameters as Fig. 2. The general behavior remains remarkably similar to Fig. 2b, with the exception that the wave period is about half of the first case.

It is pertinent to compare the predicted growth rates between the Hall mode and DKI. The range of k_y corresponding to Figs. 2 and 3 is $1.5-3\times10^{-6}\,\text{m}^{-1}$. The temperature T_0 corresponding to $B_0=50\,\text{nT}$ and $n=1\,\text{cm}^{-3}$ is $T_0=10^{-15}\,\text{J}$. The drift speed is thus calculated to be $250\,\text{km/s}$, roughly $1/3$ of the thermal speed. The growth rate predicted by Eq. (2) is then between 0.0087 and $0.0174\,\text{s}^{-1}$. The growth time range

is 58 to 115 s, much longer than the 15–20 s range shown in Figs. 2 and 3, as well as the actually observed timescale of local current disruption. Note further that that the result from Eq. (2) is an upper limit to the actual DKI growth rate (see Fig. 2 of Daughton, 1999). Another comparison is with Fig. 3 of Lapenta and Brackbill (1997). The drift-to-thermal speed ratio underlying our Figs. 2 and 3 is at the low end of the curve. The m_i/m_e ratio is about 10 times the actual value. If we apply the scaling relationship in Eq. (2) to account for the real mass ratio and $T_e=0$, an extrapolated $\gamma\sim8\times10^{-3}\Omega_i$ is obtained. For $\Omega_i\sim5\,\text{s}^{-1}$, the predicted e-folding time of DKI growth is $\sim25\,\text{s}$. It is noted, however, that this corresponds to the k_y value that maximizes the growth rate. The k_y range in Figs. 2 and 3 is somewhat off this value ($\sim5\times10^{-5}\,\text{s}^{-1}$ according to Eq. (1) and the parameters used for the figures). It is therefore safe to say that the Hall mode, for conditions representative of the magnetospheric TCS, grows as fast as, if not faster than, the DKI.

5 Discussion

This work was motivated by the question why some TCSs can stay stable for many minutes while others disintegrate in seconds. Recent observation that an electrostatic field of several mV/m precedes local current disruptions further led us to investigate the role this field might play in the destabilization of TCS. Another motivation stemmed from our analysis of the drift-kink instability. It was found that analytic results widely used for the growth rate of DKI did not include the effect of the Hall term in the generalized Ohm's law. To make up for this neglect, we constructed our theory by eliminating the possibility of DKI but with a full account of the Hall effect, leading to the identification of the so-called the Hall mode, which is exclusively an ion-scale effect. The quickest way to verify that this mode is indeed a Hall effect is through Eq. (22); that is, the d^2U/dz^2 term. If one inspects the original equations in the Appendix, he will find that this term stems from the dH_x/dz term in (A1), which, upon further inspection, is a direct consequence of the Hall MHD as manifested in Eq. (9).

The fluid formalism is applicable under limited conditions. We confirm that the results shown in Figs. 2 and 3 reside within the bound of this applicability. First, the eigenfrequency ω must be small in comparison to the asymptotic ion gyrofrequency $\Omega_i = eB_0/m$. For the conditions underlying Figs. 2 and 3, $\omega \sim 0.1 \, \text{s}^{-1}$, while $\Omega_i \sim 5 \, \text{s}^{-1}$. Second, the same eigenfrequency must be small compared to the ion bounce frequency in the magnetic field, given by $\Omega_b \sim V_{Ti}/\sqrt{LR_i}$, where $R_i = mV_{Ti}/eB_0$ is the asymptotic thermal ion gyroradius. For the parameters underlying Figs. 2 and 3, $V_{Ti} \sim 700 \, \text{km/s}$, giving $R_i \sim 140 \, \text{km}$. The resulting $\Omega_b \sim 2 \, \text{s}^{-1}$ indeed far exceeds ω. Third, the thermal ion gyroradius must be small compared to the thickness of the Harris sheet. The relevant comparison in Figs. 2 and 3 is between 140 km for R_i and 1000 km for L. Lastly, the azimuthal wavelength must be long compared to the thermal gyroradius. For Figs. 2 and 3, the wavelength ranges between 2000 and 4000 km, again meeting the constraint. Therefore, at least for the examples we used to demonstrate the Hall mode, the fluid approach is valid.

It is noted that the presence of a finite B_z can change the character of the problem and elicit new modes. In this situation, the bounce motion is no longer that associated with the meandering motion of particles about the neutral sheet, but that with mirror point reflection. The proper condition for the validity of a fluid treatment in this case would be $\omega > \omega_b$. The ion bounce frequency for a magnetic bottle geometry is approximately $B_z V_{Ti}/2B_0L$. For the same ion thermal speed and half current sheet thickness as above and for $B_z/B_0 \sim 0.1$, the bounce frequency is $\sim 0.03 \, \text{s}^{-1}$, less than $\omega \sim 0.1 \, \text{s}^{-1}$. However, the electron bounce frequency is typically faster than the wave frequency. In this paper, we took the electron temperature to be zero, and this problem was suppressed. In reality, electrons have a finite temperature.

The effect of electron terms is beyond the scope of this study and remains to be evaluated.

It is also possible for a TCS to contain a finite guide field B_y. The correction associated with B_y is on the order B_y/B_0, hence more significant than B_z. Inclusion of B_y would generalize the eigenvalue problem (20) into a fourth-order differential equation, instead of the current order of two. Solution of the generalized equation is another future interest.

In this paper, we took the limit $k_x = 0$ along the tail. If k_x is retained, the reduction of the problem would lead to another fourth-order differential equation. Some problems of interest to the substorm problem can only be studied with $k_x \neq 0$. For example, wave propagation speed in x cannot be calculated without k_x; the field-aligned currents vanish as well. A more general treatment with finite k_x will be attempted elsewhere.

Some other potential future work includes the relaxation of the $m_e \to 0$ limit to allow a unified treatment of the DKI and Hall mode and a kinetic study of the Hall mode based on the Vlasov equation.

In Fig. 1, the electric field was ascribed with a neutral-sheet point sense. This was based on the expectation, often observed, that the drift balance condition should be broken with an electron bias (i.e., $|U_e/T_e| > U_i/T_i$). However, there can be situations in which the neutral sheet is positively charged. For instance, ions can be trapped longer in the neutral sheet in some Speiser-type orbits, while electrons largely execute bounce motions. As we mentioned in respect to Eq. (30), the Hall mode can be destabilized with a negative sign of d^2U/dz^2, which corresponds to an electric field pointing away from the neutral sheet. In fact, Fig. 3, albeit of a different origin, has a second-order derivative of this sense. Hence, the Hall mode, in principle, can be excited in a positively charged neutral sheet as well. Finally we note that our result is invariant under the Galilean transformation, as adding a constant U_0 to U in our equations do not change dU/dz, and d^2U/dz^2.

The origin of the electric field that gives rise to d^2U/dz^2 is ascribed to a separation of ion and electron current sheets. The parameters in Figs. 2 and 3 were chosen from THEMIS observations of current sheet disruption. At these values, the asymptotic ion gyroradius is about 14% of the half thickness of the current sheet. At this scale, the aforementioned drift balance can be broken in the electrons' favor, and a detailed calculation (which is out of the scope of this paper) shows that an electric field of a few mV/m can arise.

The result that a TCS can become unstable with a significant temperature gradient offers an interesting prediction for future verification: the stable TCS should have more or less uniform temperature profile. When, however, the TCS starts to interact with the colder embedding plasma sheet, strong temperature gradients may develop, leading to current disruption.

The role the Hall mode plays in the substorm dynamics holds significant interest. Observational evidence suggests that magnetospheric substorms originate in the transitional

region where the magnetic field geometry changes from dipole-like to tail-like (Lui and Burrows, 1978; Samson, 1992). In this region, magnetic field lines are not quite stretched into a thin current sheet configuration, and the condition is not quite ideal for the Hall mode. Instead, many researchers believe that the region is more susceptible to the destabilization of the ballooning mode. The destabilizing term in the ballooning mode is given by $\kappa_c dp/dx$, where κ_c is the curvature of radius of field line and dp/dx the pressure gradient in equatorial plane. This term is expected to maximize in the transition region. For example, the calculation of Cheng and Zaharia (2004) put the maximal growth rate of ballooning occurs at approximately $6 R_E$. It has been proposed in the literature that perturbations from ballooning propagate outward and destabilize the current sheet in a domino effect (e.g., Ohtani et al., 1992). In the substorm event of 13 March 2007 studied by Donovan et al. (2008), three THEMIS probes were spaced by a fraction of R_E at $\sim 8.5\,R_E$, allowing a direct estimate of the propagation speed at ~ 100 km/s (or $1\,R_E$/min), 1/10 of the fast mode speed. Tailward expansion of the ballooning mode at the slower propagation speed would take about 10 min to cover $10\,R_E$, more consistent with the average duration of the expansive phase measured by geomagnetic indices and auroral activity. An important future work is to study how the passage of the ballooning mode (i.e., rarefaction wave) interacts with the local current sheet, to give rise to the destabilizing electrostatic field.

6 Conclusions

A new mode of thin current sheet dynamics was investigated in this paper. The origin of the mode is closely connected to the Hall term in the generalized Ohm's law. For reasonable parameters representing the magnetospheric TCS, the mode has a growth timescale of 10–20 s, when the current sheet thickness and azimuthal wavelength approach 1000 km. It was verified, a posteriori, that the mode satisfies the condition of two-fluid treatment. Our analysis indicated that the Hall mode is distinct from and complementary to the drift-kink instability. For the parameters chosen to reproduce the observed local current disruptions, the Hall mode appears to grow faster than the DKI, suggesting that it can be the dominant mechanism of local current disruption. Unlike the DKI, which grows in a classical Harris sheet, the Hall mode can be destabilized only when there is a significant departure from the Harris sheet, particularly a violation of the constant plasma drift across the thickness leading to a significant second-order derivative in z. This violation can be effected by either an electric field along z or a variation of the temperature across the current sheet. In the first scenario, the critical E_z is estimated to be 4 mV/m. Observations have shown that this field indeed appears a few minutes prior to local current disruption. This electric field could be the effect of a rarefac-

tion wave excited by instabilities such as ballooning occurring at an earthward location, which, in its wake, thins the current sheet to such an extent that charge separation starts to develop between the ion and electron current sheets. Details of this proposed linkage were not part of this study and requires future attention.

Appendix A

Equations (4), (6), (7), and (9) are linearized in first-order quantities, namely the magnetic field perturbations ΔB_x, ΔB_y, and ΔB_z, velocity perturbations Δu_x, Δu_y, and Δu_z, and the pressure perturbation Δp. All linear variables are ascribed with the harmonic form $\exp i\,(k_y y - \omega t)$. After straightforward manipulations, we obtain the following equations for perturbations of the form $f\,(z)\exp\left(ik_y y - i\omega t\right)$. The Faraday Eq. (9) gives the three components of the magnetic perturbation

$$\Delta B_x = \frac{k_y H_x}{\omega_d}\Delta u_y - \left(\frac{i}{\omega_d}\frac{dH_x}{dz} + \frac{imk_y}{e}\right)\Delta u_z$$
$$+\frac{m}{e}\frac{\partial \Delta u_y}{\partial z} - \frac{iH_x}{\omega_d}\frac{\partial \Delta u_z}{\partial z} \tag{A1}$$

$$\Delta B_y = -\frac{m}{e}\frac{\partial \Delta u_x}{\partial z} \tag{A2}$$

$$\Delta B_z = \frac{ik_y m}{e}\Delta u_x \tag{A3}$$

where

$$\omega_d = \omega - k_y U \tag{A4}$$

The cross product $\nabla p \times \nabla n$ vanishes for the polytropic index $\lambda = 1$.

The pressure perturbation is obtained from Eq. (7) as

$$\Delta p = -\frac{i}{\omega_d}\left[\frac{dp}{dz}\Delta u_z + ipk_y\Delta u_y + p\frac{\partial \Delta u_z}{\partial z}\right] \tag{A5}$$

The three components of the momentum equation are written as

$$-i\rho\omega_d\Delta u_x = \frac{1}{\mu_0}\frac{\partial B_x}{\partial z}\Delta B_z \tag{A6}$$

$$-i\rho\omega_d\Delta u_y + \rho\frac{dU}{dz}\Delta u_z = -ik_y\left(\Delta p + \frac{B_x\Delta B_x}{\mu_0}\right) \tag{A7}$$

$$-i\rho\omega_d\Delta u_z = -\frac{\partial}{\partial z}\left(\Delta p + \frac{B_x\Delta B_x}{\mu_0}\right) \tag{A8}$$

Substituting Eq. (A3) into Eq. (A6), it is readily verified that $\Delta u_x = 0$. By virtue of Eqs. (A3) and (A4), $\Delta B_y = \Delta B_z = 0$.

Substituting Eqs. (A1) and (A5) into Eq. (A7) yields,

$$\frac{ik_y m B_x}{\mu_0 e} \frac{\partial \Delta u_y}{\partial z} + k_y \left(\frac{\rho c_f^2}{\omega_d} - \frac{B_x m}{\mu_0 e} \frac{dU}{dz} \right) \frac{\partial \Delta u_z}{\partial z}$$

$$+ \left(\frac{i c_f^2 \rho k_y^2}{\omega_d} - \frac{i k_y^2 B m}{\mu_0 e \omega_d} \frac{dU}{dz} - i \rho \omega_d \right) \Delta u_y$$

$$+ \left(\rho \frac{dU}{dz} + \frac{m B_x k_y^2}{\mu_0 e} - \frac{m B_x k_y}{\mu_0 e \omega_d} \frac{d^2 U}{dz^2} \right) \Delta u_z$$

$$= 0 \qquad (A9)$$

while substituting Eq. (A7) into Eq. (A8) gives

$$\rho \omega_d \frac{\partial \Delta u_y}{\partial z} + i \rho \frac{dU}{dz} \frac{\partial \Delta u_z}{\partial z} + \frac{d(\rho \omega_d)}{dz} \Delta u_y$$

$$+ i \left[\frac{d}{dz} \left(\rho \frac{dU}{dz} \right) - \rho \omega_d k_y \right] \Delta u_z = 0 \qquad (A10)$$

In the case of a classical Harris sheet, $dU/dz=0$. Equation (A10) then yields Δu_z as a function of $d(\rho \Delta u_y)/dz$. Further substitution into Eq. (A9) gives Eq. (14) of the text. In the general case, one can manipulate Eqs. (A9) and (A10) by eliminating one of the first-order derivatives. Then, Δu_y can be written as a linear combination of Δu_z and du_z/dz. Elimination of Δu_y in this way leads to Eq. (20) of the text.

References

Asano, Y., Mikai, T., Hoshino, M., Saito, Y., Hayakawa, H., and Nagai, T.: Statistical study of thin current sheet evolution around substorm onset, J. Geophys., Res., 109, A05213, doi:10.1029/2004JA010413, 2004.

Birn, J., Schindler, K., and Hesse, M.: Thin electron currents and their relation to auroral potentials, J. Geophys. Res., 109, A02217, doi:10.1029/2003JA010303, 2004.

Cheng, C. Z. and Lui, A. T. Y.: Kinetic Ballooning Instability for Substorm Onset and Current Disruption Observed by AMPTE/CCE, Geophys. Res. Lett., 25(21), 4091–4094, 1998.

Cheng, C. Z. and Zaharia, S.: MHD ballooning instability in the plasma sheet, Geophys. Res. Lett., 31, L06809, doi:10.1029/2003GL018823, 2004.

Dahlburg, R. B., Antiochos, S. K., and Zang, T. A.: Secondary instability in three-dimensional magnetic reconnection, Phys. Fluids B, 4, 3902–3914, 1992.

Daughton, W.: Two-fluid theory of the drift-kink instability, J. Geophys. Res., 104, 28701–28707, 1999.

Donovan, E. F., Liu, W. W., Liang, J., et al.: Simultaneous THEMIS in-situ and auroral observations of a small substorm, Geophys. Res. Lett., 35, L17S18, doi:10.1029/2008GL033794, 2008.

Hameiri, E., Laurent, P., and Mond, M.: The ballooning instability in space plasmas, J. Geophys. Res., 96, 1513–1526, 1991.

Krall, N. A. and Trivelpiece, A. W.: Principles of Plasma Physics, p. 91, McGraw-Hill, New York, 1973.

Lapenta, G. and Brackbill, J. U.: A kinetic theory for the drift-kink instability, J. Geophys. Res., 102, 27099–27108, 1997.

Lee, L.-C., Zhang, L., Choe, G. S., and Cai, H. J.: Formation of a very thin current sheet in the near-Earth magnetotail and the explosive growth phase of substorms, Geophys. Res. Lett., 22, 1137–1140, 1995.

Liang, J., Donovan, E. F., Liu, W. W., et al.: Intensification of preexisting auroral arc at substorm expansion phase onset: Wave-like disruption during the first tens of seconds, Geophys. Res. Lett., 35, L17S19, doi:10.1029/2008GL0336666, 2008.

Liang, J., Liu, W., Donovan, E., and Spanswick, E.: In-situ observation of ULF wave activities associated with substorm expansion phase onset and current disruption, Ann. Geophys., in review, 2009.

Liu, W. W.: Disruption of thin current sheets: A two-fluid theory, J. Geophys. Res., 102, 14331–14341, 1997a.

Liu, W. W.: Physics of the explosive growth phase: Ballooning instability revisited, J. Geophys. Res., 102, 4927–4931, 1997b.

Liu, W. W., Liang, J., and Donovan, E. F.: Interaction Between Kinetic Ballooning Perturbation and Thin Current Sheet: Quasi-Electrostatic Field, Local Onset, and Global Characteristics, Geophys. Res. Lett., 35, L20107, doi:10.1029/2008GL035757, 2008.

Lui, A. T. Y.: A synthesis of magnetospheric substorm models, J. Geophys. Res., 96, 1849–1856, 1991.

Lui, A. T. Y. and Burrows, J. R.: On the location of auroral arcs near substorm onsets, J. Geophys. Res., 83, 3342–3348, 1978.

Mitchell, D. G., Williams, D. J., Huang, C. Y., Frank, L. A., and Russell, C. T.: Current carriers in the near-Earth cross-tail current sheet during substorm growth phase, Geophys. Res. Lett., 17, 583–586, 1990.

Ohtani, S., Kokubun, S., and Russell, C. T.: Radial expansion of the tail current disruption during substorms: A new approach to the substorm onset region, J. Geophys. Res., 97, 3129–3136, 1992.

Pritchett, P. L. and Coroniti, F. V.: Formation of thin current sheets during plasma sheet convection, J. Geophys. Res., 100, 23551–23565, 1995.

Pritchett, P. L., Coroniti, F. V., and Decyk, V. K.: Three-dimensional stability of thin quasi-neutral current sheets, J. Geophys. Res., 101, 27413–27429, 1996.

Pulkkinen, T. I., Baker, D. N., Cogger, L. L., Frank, L. A., Sigwarth, J. B., Kokubun, S., Mukai, T., Singer, H. J., Slavin, J. A., and Zelenyi, L.: Spatial extent and dynamics of a thin current sheet during the substorm growth phase on December 10, J. Geophys. Res., 104, 28475–28490, 1999.

Roux, A., Perrault, S., Robert, P., Morane, A., Pedersen, A., Korth, A., Kremser, G., Aparicio, B., Rodgers, D., and Pellinen, R.: Plasma sheet instability related to the westward traveling surge, J. Geophys. Res., 96, 17697–17714, 1991.

Runov, A., Sergeev, V. A., Nakamura, R., et al.: Local structure of the magnetotail current sheet: 2001 Cluster observations, Ann. Geophys., 24, 247–262, 2006,
http://www.ann-geophys.net/24/247/2006/.

Saito, M. H., Miyashito, Y., Fujimoto, M., et al.: Ballooning mode waves prior to substorm-associated dipolarizations: Geotail observations, Geophys. Res. Lett., 35, L07103, doi:10.1029/2008GL033269, 2008a.

Saito, M. H., Miyashita, Y., Fujimoto, M., Shinohara, I., Saito, Y., and Mukai, T.: Modes and characteristics of low-frequency MHD waves in the near-Earth magnetotail prior to dipolarization: Fitting method, J. Geophys. Res., 113, A06201, doi:10.1029/2007JA012778, 2008b.

Samson, J. C., Lyons, L. R., Newell, P. T., Creutzberg, R. F., and Xu, B.: Proton aurora and substorm intensifications, Geophys. Res. Lett., 21, 2167–2170, 1992.

Sanny, J., McPherron, R. L., Russell, C. T., Baker, D. N., Pulkkinen, T. I., and Nishida, A.: Growth-phase thinning of the near-Earth current sheet during the CDAW 6 substorm, J. Geophys. Res., 99, 5805–5816, 1994.

Schindler, K. and Birn, J.: Models of two-dimensional embedded thin current sheet from Vlasov theory, J. Geophys. Res., 107, 1193, doi:10.1029/2001JA000304, 2002.

Sergeev, V. A., Mitchell, D. G., Russell, C. T., and Williams, D. J.: Structure of the tail plasma/current sheet at $\sim$11 R_E and its changes in the course of a substorm, J. Geophys. Res., 98, 17345–17365, 1993.

Sitnov, M. I., Zelenyi, L., Malova, H. V., and Sharma, A. S.: Thin current sheet embedded within a thicker plasma sheet: Self-consistent theory, J. Geophys. Res., 105, 13029–13043, 2000.

Zhu, Z. and Winglee, R. M.: Tearing instability, flux ropes, and the kinetic current sheet kink instability in the Earth:s magnetotail: A three-dimensional perspective from particle simulations, J. Geophys. Res., 101, 4885–4897, 1996.